A comparative study of natural gas and biogas combustion in a swirling flow gas turbine combustor

Journal:	*Combustion Science and Technology*
Manuscript ID	GCST-2020-0352.R1
Manuscript Type:	Full Manuscript
Date Submitted by the Author:	18-Dec-2020
Complete List of Authors:	Rahman, Tariq M. R.; International Islamic University Malaysia, Mechanical Engineering Hoda, Asif; Jubail University College, Mechanical Engineering Asrar, Waqar; International Islamic University Malaysia, Mechanical Engineering Khan, Sher Afghan; International Islamic University Malaysia, Mechanical Engineering
Keywords:	Biogas and natural gas combustion, Alternative fuel, Combustion performance, Swirl number, Fuel injector

A comparative study of natural gas and biogas combustion in a swirling flow gas turbine combustor

Tariq M. R. Rahman[a], Asif Hoda[b,*], Waqar Asrar[a], Sher Afghan Khan[a]

[a]*Department of Mechanical Engineering, International Islamic University Malaysia, 53100 Kuala Lumpur, Malaysia.*
[b]*Department of Mechanical Engineering, Jubail University College, Al Jubail 35716, Saudi Arabia.*

Abstract

In this study, non-premixed combustion of a traditional fuel- natural gas, and an alternative fuel- biogas, is simulated in a swirling flow industrial gas turbine combustor geometry which includes the combustor liner and the outside casing in order to replicate the flow and combustion in a real gas turbine combustor. The 3D combustion simulations are validated and the results for combustion of both gases are analyzed to compare and evaluate the viability of biogas as an alternative fuel for use in industrial gas turbine combustors. The combustion performance is evaluated based on multiple combustion performance optimization parameters, namely the combustion efficiency, pattern factor, and pollutant emissions (CO and NO). The effects of two design parameters: swirl number and fuel injector diameter on the combustion performance optimization parameters are examined. The results have been analyzed to identify the best case for each combustion performance optimization parameter and a suitable trade-off case for both gases is proposed. Additionally, the comparison of the combustion performances of both gases revealed that despite possessing much lower methane and hence lower heating value (LHV), a combination of swirl number and fuel injector diameter for biogas of a specific composition results in a combustion performance comparable to natural gas along with lower NO emission, although at the expense of higher CO emission. Therefore, biogas can potentially be utilized as an alternative fuel in industrial gas turbine combustors and methods for reducing CO emission can be devised.

Keywords: Biogas and natural gas combustion, alternative fuel, combustion performance, swirl number, fuel injector, gas-turbine emissions

1. Introduction

Gas turbine combustor design and development have been focused on achieving higher combustion efficiency, proper flame temperature and gas concentrations, lower and balanced emissions, lower pattern factor, and minimized entropy generation (Elbaz et al., 2019; Elbaz and Roberts, 2016; Jerzak and Kuźnia, 2016; Santhosh and Basu, 2016; Shanbhogue et al., 2016; Taamallah et al., 2016). Both conventional fuels like kerosene (Chmielewski and Gieras, 2017; Li et al., 2016), propane (Krieger et al., 2015; Wankhede et al., 2011), methane or natural gas, some liquid-fuels (Kahraman et al., 2018; Motsamai et al., 2010), and non-conventional fuels like biogas, hydrogen (Bothien et al., 2019; İlbaş, Karyeyen and İlker Yılmaz, 2016; Rohani and Saqr, 2012), syngas (Safer et al., 2017; Iqbal et al., 2016) have been used in gas turbine combustors. All these investigations have been conducted in different mixing uniformities such as premixed, partially-premixed and non-premixed.

*Corresponding author
Email addresses: tariq.ridwanur@live.iium.edu.my, tariq.ridwan@gmail.com (Tariq M. R. Rahman), hodaa@ucj.edu.sa, ahoda10@gmail.com (Asif Hoda), waqar@iium.edu.my (Waqar Asrar)

Due to significant usage of fossil fuel in every sector of power generation leading to environmental pollution and depletion of conventional fuels, the world is forced to move towards alternative and cleaner sources of energy. Biogas is a promising source as it can be produced from raw materials such as agricultural, animal, and municipal waste. The development of gas turbines until today is centered around fossil fuels. Increasing usage of alternative fuels like biogas in gas turbines requires investigation of the effect of the various design parameters on the gas turbine combustion optimization parameters (Masri, 2020; Lefebvre and Ballal, 2010; Murphy, 2004).

Many investigations on gas turbine combustor during the last decade have explored the performance of natural gas combustion with some reported works on biogas as well. Amani et al. (2019) proposed a mathematical model to analyze effects of different air partitioning strategies in a complex combustor configuration based on seven combustion performance parameters. They observed that the optimal design needs a large portion of total air through the primary and dome holes. The design also reduces emission by 78% while improving the efficiency by 6%. In a similar study, Emami et al. (2019) concluded that the NO_x emission is minimum if the swirl angle is 55 and it is directly related to fuel and combustion gas temperature. Another mathematical model proposed by Torkzadeh et al. (2016) analyzes the effect of swirl number on four combustion optimization parameters and found an optimal case that possesses a swirl number that is 44% smaller than the base case. The investigations of Rashwan et al. (2018) revealed that the thermal NO_x can be reduced by 95% if higher swirl number is utilized, while İlker Yılmaz (2013) found significant influence of swirl number on the formation of central and external recirculation zones, flame temperature and concentration of different gases. It is therefore clear from these investigations that the swirl number is an important design parameter and that any comprehensive investigation should study the influence of swirl number on combustion performance parameters such as pollutant emissions.

Zhang et al. (2020) analyzed the influence of different fuel mixing uniformities on the flame dynamic response in real conditions to provide support for the design of gas turbine combustor and found that both the uniform premixed and partially premixed case have the double helix vortex core structure. Yang et al. (2019) found that the semi-major/semi-minor axis ratio has significant influence on the combustion and emission performance of elliptical jet-stabilized combustors. Lellek et al. (2017) experimentally investigated the effect of water injection on swirling premixed combustion and recommended water-to-fuel ratio up to 2.25 for stable flame establishment. They further noted that the global water distribution and water droplet sizes influence NO_x emission the most. A similar investigation by Farokhipour et al. (2018) concluded that the best water injection location is at the end of the primary zone, while a combination of higher mass flow rate and higher swirl intensity gives reduced NO_x emission. This work was extended further by Amani et al. (2018) by considering additional design parameters and it was concluded that an optimal water-to-fuel ratio of 3.4, reduces the emission and temperature non-uniformity by 110% and 19%, respectively.

Shahpouri and Houshfar (2019) investigated a humid combustion case and reported minimum NO_x emission when the water-to-fuel ratio is close to 1, while better combustion efficiency and pollutant reduction are achieved if the inlet air humidity increases by 25%. Göke et al. (2014) studied the sensitivity of steam and pressure on pollutant emission and recorded a significant reduction of CO and NO_x formation at ultra-wet conditions and exponential increase in NO_x emission at dry conditions. It can be concluded from these investigations that development of pollutant reduction techniques similar to water injection maybe focused on in a combustion optimization study.

Makhanlall et al. (2013) calculated energy devaluation in the 300 kW BERL combustor (Sayre et al., 1994) through entropy generation minimization and recommended an optimum fuel-air equivalence ratio of 0.7 if natural gas is used. In the same combustor, Hajitaheri (2012) attempted to achieve maximum fuel conversion to CO_2 by changing the swirl number and quarl angle. He suggested a swirl number of 0.51 with 23.2 quarl angle instead of the initial empirical case which increased the CO_2 mass generation for about 1.66 kg/hour. Citing the importance of geometrical design parameters on the performance of micro-combustors, Ansari and Amani (2018) proposed a novel combined baffle-bluff assembly that improved average temperature by 6.3% and uniformity by 87.5%. They noted that the combustion efficiency and entropy generation rate are heavily influenced by the baffle length and wall conductivity, respectively. The optimization by Iki et al. (2007) displayed considerable improvement in micro gas turbine combustor operation by inverting air flow ratio between the inner and outer liner of the combustor. It can therefore be inferred that geometrical parameters have been observed to have significant influence on combustion performance.

Asgari and Amani (2017) investigated the influence of four fuel injection design parameters on performance of a modern dry-low-emission premixed gas turbine combustor. They observed that the location and direction of fuel injection plays a significant role on the evaporation efficiency, and the interactions between the spray and the two swirling vortices in the chamber strongly affect the mixture stratification. Burmberger and Sattelmayer (2011) provided an aerodynamic design guideline that renders maximum safety against flashback which occurs due to vortex breakdown induced during lean-premixed swirl-stabilized natural gas combustion. Fuligno et al. (2009) studied the influence of position and size of the liner holes and exit duct on NO_x emission and pattern factor. Fully premixed methane combustion in a 150-kW burner by Bhoi and Channiwala (2008) revealed that uniform and stable flame is achieved with a conventional bluff body with a 0.65 blockage ratio and the burner flammability limit is established in the range of 40-55%. Therefore, proper fuel injector design becomes of significant importance while designing gas turbine combustors.

Sahebjamei et al. (2019) noted improved combustion efficiency and pattern factor after imposing a combined radial-angular stratified condition during methane-air combustion. Rajabi and Amani (2018) observed a 25% rise of entropy generation due to radiation in a methane-air diffusion flame for a range of swirl numbers. Arjmandi and

Amani (2015) calculated entropy generation using two different methods and found the results differ by 6%, while chemical reaction and heat transfer are the main contributors behind entropy generation and their trade-off results in the optimum design condition. In a similar study, Janiga and Thévenin (2007) investigated CO emission minimization by varying the fuel-air ratio in primary and secondary outlet. These investigations seem to suggest that parameters like combustion efficiency and pattern factor maybe utilized to asses the feasibility of using alternate fuels in gas turbine combustors.

Similar investigations have also been conducted using biogas, among them the recent investigation by Şahin (2019) analyzed the thermal field distributions and pollutant emission in combustion of several biogases of different compositions under distributed combustion conditions in an existing natural gas burner. The result showed good agreement with the experimental data. For the biogas with lower oxygen concentration, nearly zero emissions were predicted for CO and NO_x emission while CO_2 level increased slightly. Şahin and İlbaş (2019) further examined the influence of H_2O amount on the combustion of H_2S- and H_2O- containing biogas using the same burner and concluded that higher H_2O content provides lower SO_2 and CO emission. Therefore it can be deduced that the composition of biogas and the presence additives like H_2O have a significant influence on the emissions.

Several non-premixed and premixed combustion of biogas in industrial burner with higher H_2 content have been reported in the published literature (Hosseini and Wahid, 2014; Zhen, Leung and Cheung, 2014; Zhen, Leung, Cheung and Huang, 2014; Zhen et al., 2013) and the results demonstrated higher combustion stability and flame temperature level. Consequently, CO emission decreased while entropy generation and NO_x emission increased. In addition, it was reported that the lower heating value (LHV) of biogas increases with higher H_2 content. The effect of CO_2 content in biogas on CO formation for non-premixed and premixed combustion in burners and modeled combustors have also been investigated in multiple studies (Fischer and Jiang, 2017; Khaleghi et al., 2015; Mordaunt and Pierce, 2014) and the results indicated that higher CO_2 content leads to lower flame stability and temperature, and hence higher CO emission. In a similar study (Guessab et al., 2016), a monotonous NO_x reduction with increasing CO_2 content in biogas has also been reported. The combustion characteristics of biogas can therefore be altered by varying H_2 and CO_2 contents.

Chen et al. (2017) proposed a newly designed enhanced lean premixed nozzles for hydrogen-enriched biogas combustion in a model micro gas turbine combustor and found the nozzles performed better than the original one and caused strong swirl intensity and vortices at their outlet which contributed to enhanced mixing of air and fuel. Another experimental investigation (Saediamiri et al., 2016) in a burner concluded that the fuel nozzle diameter and discharge angle drastically influence the stability of biogas swirling non-premixed and premixed flame and pollutant CO emission. Other studies (Leung and Wierzba, 2008, 2007) reported the influence of nozzle size on flame stability

in combustion chambers. The combustion investigation of İlbaş and Şahin (2017) in a burner concluded that higher turbulator angle results in better air-fuel mixture, thereby resulting in significant increase in combustion completeness and CO_2 emission. Birouk et al. (2014) found in their experimental investigation that the flame attached to high swirl in a burner stabilizes a wide range of flow conditions compared to low swirl attached flame. Effuggi et al. (2008) analyzed NO_x, soot and Polycyclic Aromatic Hydrocarbons (PAHs) emissions for premixed biogas combustion in a burner and found that mild combustion can be used for a wide range of low-BTU fuels, and is able to reduce NO_x, soot and PAHs emissions. Flame stability and emissions seem to have a close dependence on the nozzle diameter and size.

Experimental and numerical investigations (İlbaş, Şahin and Karyeyen, 2018, 2016) on combustion of methane and four different compositions of biogas in an industrial burner have found that one of the four biogases demonstrate temperature distribution and maximum flame temperature very close to methane. Biogas flameless combustion in burners and furnaces were investigated experimentally and numerically (Hosseini and Wahid, 2015; Hosseini et al., 2014; Hosseini and Wahid, 2013) and it was found that the temperature distribution was more uniform for flameless combustion, while the combustion efficiency was 53% compared to 32% for the conventional combustion. Furthermore, tangential burner configuration performs better than coaxial configurations for flameless combustion. Despite that, combustion wall heat loss for tangential burner configuration was higher than the coaxial ones. Although biogas has been found to have combustion performance close to methane in burners and furnaces, it remains to be seen whether similar trends can be achieved in an actual gas turbine combustor.

The literature survey conducted in this study shows that although a number of natural gas and biogas combustion studies have been reported, investigations involving actual gas turbine combustor geometries and comparative combustion performance analysis of natural gas and biogas have received little attention in published literature. Therefore, the present study targets the simulation, analysis and comparison of natural gas and biogas combustion in a gas turbine combustor designed by the authors. A combustion analysis of the influence of the swirl number and the fuel injector diameter on the combustion efficiency, pattern factor (PF), and pollutant CO and NO emissions is the main focus of this study. Additionally, a comparison of the combustion performance of natural gas and biogas combustion is also targeted to assess the feasibility of the use of biogas in industrial gas turbine combustors.

2. Mathematical model

2.1. Combustor geometry

A gas turbine combustor designed based on standard combustor design methodology and empirical formulations, considering the practical aspects of combustor design (Melconian and Modak, 1985; Conrado et al., 2004) for swirling

flow non-premixed combustion is shown in Figures 1 and 2. The combustor design specifications are given in Table 1. Simulations in the present work are conducted in 3D using the FLUENT code, as the swirling flow and its substantial role in the mixing process during combustion is highly 3D in nature. In addition, unlike the investigations in the existing literature, the annulus between the casing and liner is included in the simulations to realistically predict the path of the incoming airflow from the annulus and flowing into the different holes and cooling slots. The computational domain is shown in Figure 2.

2.2. *Composition of gases*

Biogas of different compositions have been investigated in published literature and it has been observed that significant presence of CO_2 in biogas causes reduction in peak pressure, combustion stability and heat generation, and increased CO emission, while biogas containing more than 45% CO_2 causes harsh and irregular functioning of the engine (Fischer and Jiang, 2017; Khaleghi et al., 2015; Mordaunt and Pierce, 2014; Leung and Wierzba, 2008, 2007). Hobson et al. (1981) and Biswas (1994) reported increased unburned fuel emission in the range of 45-50% CO_2. Therefore, biogas with high CO_2 concentration must be avoided for better performance and pollutant emission minimization. The recommended biogas by İlbaş, Şahin and Karyeyen (2018) for use in industrial combustors as an alternative fuel to natural gas mainly consists of 33% CO_2 and 65% CH_4. Similar composition has also been recommended by Liguori (2016). Based on the recommendations in published literature, the compositions of natural gas and biogas used in this study are listed in Table 2. The stoichiometric air-fuel ratio of the biogas used in this study is calculated as 7:1. For natural gas, a standard value of 17.2:1 (Heywood, 1988) was adopted. 10% excess air was used to achieve highest possible efficiency as recommended by Kuznetsov (1973). The significant difference in stoichiometric air-fuel ratio of natural gas and biogas indicates why a higher amount of fuel (and therefore higher fuel velocity) is required for biogas combustion for the same air-flow rate and fuel injector diameter (see Table 1).

2.3. *Governing equations*

The governing equations comprise of continuity and momentum as listed below:

$$\frac{\partial}{\partial x_i}(\rho u_i) = 0 \tag{1}$$

$$\frac{\partial}{\partial x_j}\left(\rho u_i u_j\right) = -\frac{\partial p}{\partial x_i} + \frac{\partial}{\partial x_j}\left[\mu\left(\frac{\partial u_i}{\partial x_j} + \frac{\partial u_j}{\partial x_i} - \frac{2}{3}\delta_{ij}\frac{\partial u_l}{\partial x_l}\right)\right] + \frac{\partial}{\partial x_j}\left(-\rho\overline{u_i' u_j'}\right) \tag{2}$$

The closure for the Reynolds stresses $-\rho\overline{u_i' u_j'}$ is specified by the Boussinesq approximation

$$-\rho\overline{u_i' u_j'} = \frac{2}{3}k\delta_{ij} + \mu_t\left(2S_{ij}\right) \tag{3}$$

where,

$$S_{ij} = \frac{1}{2}\left(\frac{\partial u_i}{\partial x_j} + \frac{\partial u_j}{\partial x_i}\right) \tag{4}$$

The turbulent viscosity μ_t is specified in the standard $k-\epsilon$ model as follows:

$$\mu_t = \rho c_\mu f_\mu \frac{k^2}{\epsilon} \tag{5}$$

Here, c_μ has a standard value of 0.09 and $f_\mu = 1$ for the standard wall function model. Additionally, a number of different formulations for the function f_μ are also available in published literature (Launder and Spalding, 1974; Lam and Bremhorst, 1981). The kinetic energy k and the turbulent dissipation rate ϵ are determined by solving their respective transport equations (Launder and Spalding, 1974). Heat transfer is handled by solving the Energy equation (Patankar, 1980). For turbulence-chemistry interaction, the non-premixed steady-flamelet model (Pitsch and Peters, 1998; Peters, 2004; Poinsot and Veynante, 2005) is used based on primitive variables, where the temperature T, and the mean of local mass fraction of species Y_i, are obtained from lookup tables generated as functions of the mean mixture fraction f, its variance f'^2, and mean scalar dissipation χ_{st}. For lookup tables, the transport equations for f and f'^2, are solved as,

$$\frac{\partial}{\partial t}(\rho f) + \frac{\partial}{\partial x_j}(\rho u_i f) = \frac{\partial}{\partial x_j}\left(\frac{\mu_t}{\sigma_t}\frac{\partial f}{\partial x_j}\right) \tag{6}$$

$$\frac{\partial}{\partial t}\left(\rho f'^2\right) + \frac{\partial}{\partial x_j}\left(\rho u_i f'^2\right) = \frac{\partial}{\partial x_j}\left(\frac{\mu_t}{\sigma_t}\frac{\partial f'^2}{\partial x_j}\right) + C_g \mu_t \left(\frac{\partial f}{\partial x_j}\right)^2 - C_d \rho \frac{\epsilon}{k} f'^2 \tag{7}$$

where, μ_t is the turbulent viscosity. The values for the constants σ_t, C_g, C_d are 0.85, 2.86, and 2.0 respectively. The mean scalar dissipation is modeled as,

$$\chi_{st} = \frac{C_\chi \epsilon f'^2}{k} \tag{8}$$

here C_χ is a constant with a value of 2.

2.4. Combustion parameters

2.4.1. Swirl number

The swirl number is one of the most important design parameters (Farokhipour et al., 2018; Rajabi and Amani, 2018; Torkzadeh et al., 2016) and is defined as the ratio of the axial flux of the tangential or swirl momentum and the axial flux of the axial momentum multiplied by a characteristic length R,

$$S = \frac{\int_0^R UWr^2 dr}{R\int_0^R U^2 r dr} \tag{9}$$

where W and U are the mean axial and tangential velocity respectively, at the exit plane of the swirl generator. However, in the present work, the level of swirl is characterized by the geometric swirl number, $S_g = U_s/W_s$, defined according to Kalt et al. (2002). Here, W_s and U_s are the bulk axial and tangential velocity of the swirling air stream. The actual swirl number is linearly proportional to the geometric swirl number ($S = 0.90S_g$) which can be varied by changing the relative magnitudes of the tangential and axial airflow rates (Al-Abdeli and Masri, 2003).

In the current study, swirl numbers: 0.5, 0.9, 1.5, and 2.0 are considered to account for half, one, one and a half, and double swirl intensities respectively. Swirl numbers less than 0.5 are not tested, as Lefebvre and Ballal (2010) stated that values less than 0.4 produce no recirculation zones and such swirls are defined as weak. Therefore, swirlers of practical interest operate with a strong swirl, which is typically above swirl number 0.6.

2.4.2. Fuel injector diameter

Fuel injector diameter is a sensitive design parameter which influences flame stabilization and pollutant emission (Saediamiri et al., 2016; Mordaunt and Pierce, 2014). Changes in the fuel injector diameter changes the velocity of the incoming fuel and also influences the thickness of the separator between the swirler and fuel injector. For large injector diameter, the separator is a wall, while for lower injector diameter the separator acts as a bluff body. The bluff-body thickness has crucial impact on the formation and shape of various recirculation zones in different locations inside the combustor which controls the mixing process. Fuel injector with three different diameters are considered as design parameters in the present work, as listed in Table 3.

2.4.3. Combustion efficiency

Combustion efficiency and pattern factor are the conventional combustion performance parameters used since the early days of gas turbine engine development (Mattingly et al., 2002). The combustion efficiency typically measures combustion completeness (Boyce, 2012) which directly affects fuel consumption, as unburned fuels heating value is not utilized to increase combustion gas temperature. Lower efficiency also leads to pollutant emissions such as carbon monoxide (CO) and unburned hydrocarbon (UHC) (Lefebvre and Ballal, 2010). The combustion efficiency is defined by the ratio of the actual heat release of the gas and the maximum possible theoretical heat input of the fuel (Boyce, 2012; Mattingly et al., 2002; Razak, 2007). Mathematically,

$$\eta_c = \frac{\Delta h_{actual}}{\Delta h_{theoretical}} = \frac{\sum_{outlets} \dot{m} h_s - \sum_{inlets} \dot{m} h_s}{\dot{m}_f Q_f} \tag{10}$$

where, h_s is the mixture sensible enthalpy, $\dot{m}$ is the mass flow rate in or out of the combustor, $\dot{m}_f$ is fuel mass flow rate, and Q_f is the lower heating value of the fuel. The mixture sensible enthalpy is defined as,

$$h_s = \sum_i Y_i h_i + \frac{p}{\rho} \tag{11}$$

where Y_i is the mass fraction of species i and $h_i = \int_{T_{ref}}^{T} c_{p,i} dT$ with reference temperature $T_{ref} = 298$ K.

2.4.4. Pattern factor

Higher uniformity of the combustor outlet temperature profile ensures longer life of the turbine nozzle vane. Conventionally, non-uniformity of the combustor outlet temperature profile is calculated using,

$$PF = (T_{max,outlet} - T_4) / (T_4 - T_3) \tag{12}$$

here PF is the pattern factor, defined as the difference between maximum combustor outlet temperature ($T_{max,outlet}$) and the mean combustor outlet temperature (T_4) normalized by the mean temperature rise in combustor ($T_4 - T_3$) (Mattingly et al., 2002; Torkzadeh et al., 2016).

2.4.5. Pollutant emission

The formation of the Pollutant CO and NO are calculated using the mixture fraction, f, defined in terms of the atomic mass fraction by Sivathanu and Faeth (1990):

$$f = \frac{Y_i - Y_{i,ox}}{Y_{i,fuel} - Y_{i,ox}} \tag{13}$$

where Y_i is the elemental mass fraction for element, i. The subscript ox denotes the value at the oxidizer stream inlet and the subscript $fuel$ denotes the value at the fuel stream inlet.

3. Numerical method

The Finite Volume Method (FVM) is applied to solve the governing equations along with SIMPLE algorithm for pressure-velocity coupling. Second-order upwind scheme is incorporated for the discretization of the convection term in the momentum equation and the scalar equations for the reacting flow. A no-slip boundary condition is implemented on all the walls, while the normal gradient of pressure is set equal to zero at all boundaries. Choice of reaction-mechanism plays a crucial role in combustion simulation. The GRI 3.0 and GRI 2.11 mechanisms which

include NO formation have been tested as part of the validation process. The GRI 3.0 mechanism comprised of 325 reactions and 53 species, while the GRI 2.11 contains 277 reactions and 49 species.

Although the GRI reaction-mechanism is designed for methane and natural gas combustion, it is also a viable mechanism for biogas combustion in predicting the pollutant CO and NO_x emissions, as found by Fischer and Jiang (2015). They also found that the GRI mechanism is the most reliable mechanism considering overall aspects of biogas combustion if there is no significant presence of hydrogen in the biogas. As the biogas composition used in the current work has no presence of hydrogen (see Table 2), the GRI reaction-mechanisms can be used reliably for biogas combustion.

3.1. Validation and grid-independence test

For validation, the swirling methane flame (SM1) case of the Swirl Flows and Flames Database also known as the Sydney swirl flame database is used. This is considered a reliable validation case for swirling flow combustion in an industrial type burner. The operating conditions and configuration of the Sydney swirl burner have been reported by Kalt et al. (2002) and Masri (2007). A 3D grid of 1.0 million cells is used for the simulation. The line plot comparisons of experimental measurements and computed results of the axial and tangential velocity, temperature, mean mixture fraction, and CO_2, CO, NO formations are shown in Figures 3 to 5. The axial position z is normalized by the bluff body diameter D = 50 mm, while the radial position r is normalized by the fuel inlet radius R_j = 1.8 mm. The axial velocity W and tangential velocity U are normalized by the fuel velocity W_j = 32.7 m/s and the tangential velocity of air stream through the swirler U_s = 19.1 m/s, respectively.

It can be observed from the line plots that the computed results are in good agreement with the experimental measurements. The symmetric feature of the 3D flow field, temperature distribution, pollutant formations have also been captured by the simulation. There is no visible difference in the predictions by both reaction-mechanisms except for the NO formation, where the computation by GRI 3.0 is slightly off in the first two locations (z/D = 0.4 and z/D = 0.8 in Figure 5(c)), and far-off in the last two locations (z/D = 1.1 and z/D = 1.5 in Figure 5(c)). This phenomenon of excess NO formation prediction by GRI 3.0 has also been reported by Jaravel (2016) in his comparative analysis of NO formation using GRI 3.0 and 2.11. Therefore, the GRI 2.11 reaction-mechanism is going to be used in subsequent investigations.

The 3D grid generated for the combustion investigation in a gas turbine combustor comprises of 7.36 million cells as shown in Figure 6. To check the grid sensitivity, results of the reference case (INJ-765 with S_g = 0.9) obtained using a finer grid of 14.7 million cells is compared with the results obtained using 7.36 million grid as shown in Figure 7. Results show that there is no visible and significant difference in the predictions of axial velocity and temperature.

4. Results and discussion

The result of the reference case (INJ-765 with S_g = 0.9) of natural gas combustion is examined first. The contours of the axial velocity, Y-vorticity, and turbulent kinetic energy are depicted in Figure 8 along with 2D and 3D streamlines.

Analyzing the axial velocity contour, 3D and 2D streamlines in Figures 8(a) and 8(b), it can be observed that the flow develops two internal recirculation zones (IRZ). The IRZs are counter rotating as indicated in the Y-vorticity contour in Figure 8(b). The smaller inner-IRZ is formed due to the incoming natural gas through the central fuel injector, while the bigger outer-IRZ is formed by the swirling flow through the swirler. An interesting 3D ring-like structure is observed in the outer-IRZ region as pointed out in Figure 8(a). There is a central recirculation zone (CRZ) in the middle of the combustor which is visible only through the 3D streamlines shown in Figure 8(a). The CRZ can also be observed from the turbulent kinetic energy contour in Figure 8(c), where a low turbulent kinetic energy region is visible. These recirculation zones inside the combustor liner contribute to a proper mixing of air and fuel where the swirling air flow plays a big role in the process.

The intensity of the swirling flow plays an important role in the combustion performance and has a direct influence on the different combustion optimization parameters. Figure 9(a) shows the effects of different swirl intensities on the flow pattern inside the combustor, for INJ-765 injector. It can be observed that with increasing swirl number the outer-IRZ begins to dominate over the inner-IRZ and at swirl number 2.0 the outer-IRZ is almost twice as big as the inner-IRZ which has reduced in size significantly.

The dominance of the outer-IRZ with increasing swirl number has a direct influence on the combustion as can be observed from the temperature contours in Figure 9(b). As the outer-IRZ begins to dominate over the inner-IRZ, a corresponding increase in the high temperature region is observed in the temperature contours which indicates an early onset of combustion, more complete combustion and therefore higher efficiency can be expected. This observation is very clear for S_g = 1.5 and 2.0, where large high-temperature regions can be seen covering the central regions of the combustor. The effect of the swirling airflow on the mixing of the fuel with air and subsequent combustion can be noted from the thin streaks of high-temperature observed parallel to the inclined dome-wall. However, a much lower temperature layer can be observed between the dome wall and the high-temperature streaks which is due to film-cooling air being provided by the dome cooling slots. The effect of film-cooling by combustor liner cooling slots is also clearly visible in the form of low temperature layers protecting the liner from the high-temperature regions.

The emission patterns for INJ-765 with increasing swirl numbers is shown in Figure 10. The early onset of combustion and higher combustor temperature for S_g =1.5 and 2.0 also contribute to a corresponding CO oxidation and hence lesser CO emission at the combustor exit as depicted in Figure 10(a). However, higher NO emissions are

observed at the outlet as the swirl number increases as shown in Figure 10(b).

After analyzing the reference case (INJ-765 with S_g = 0.9) in terms of flow patterns, temperature profiles (Figure 9), and CO and NO formation (Figure 10) and their variation with swirl number, a detailed analysis of the influence of swirl number on the combustion optimization parameters for different injector diameters (10.65 mm and 5.75 mm) has been carried out and compared with INJ-765 through line plots in Figure 11.

The line plots in Figure 11 provide a broader picture about the effect of the design parameters (swirl number and fuel injector diameter) on different combustion performance optimization parameters. This allows to choose a specific fuel injector and swirl number that results in a suitable trade-off between combustion efficiency, pattern factor, and pollutant emissions (CO and NO). The increase in the high-temperature region and hence more complete combustion with increasing swirl number observed for INJ-765 injector in Figure 9(b), is manifested in the form of higher efficiency and higher maximum combustor temperature for all injectors with increasing swirl number in Figure 11(a). The influence of swirl number on PF: pattern factor and T_4: mean temperature at combustor exit is depicted in Figure 11(b). It can be seen that the PF decreases with increasing swirl number for all injectors indicating higher uniformity of temperature profile at the combustor outlet and a corresponding increase in T_4 is observed for all injectors. The inverse relationship of CO and NO emission against swirl number is visible in Figure 11(c). In order to determine the balanced emission for the injectors, the intersecting points of the CO and NO lines are identified at the X-axis locations of S_g = 0.755, 0.898, and 1.215 (marked by green squares in Figure 11(c)) for the injectors INJ-1065, INJ-765, and INJ-575 respectively. It can be observed that the balanced CO and NO emissions at the intersecting points are almost equal for INJ-1065 and INJ-765, for S_g = 0.755 and 0.898 respectively, while that for INJ-575 and S_g = 1.215 is comparatively higher. Furthermore, analyzing Figure 11(d) the combustion efficiency and pattern factor for the different injectors at the location of the swirl number corresponding to balanced emissions is listed in Table 4 below.

It can be concluded based on Table 4 that INJ-765 with S_g = 0.898 (approximately 0.9) can be considered as the most suitable combination amongst the different fuel injector diameters and swirl numbers analyzed.

The flow pattern of biogas combustion using INJ-765 injector for different swirl numbers are shown in Figure 12(a). It can be observed that the higher fuel velocity in biogas combustion (compared to natural gas combustion) makes the inner-IRZ more dominant compared to the corresponding cases of natural gas combustion shown in Figure 9(a). The temperature contours in Figure 12(b) indicate that the high-temperature regions do not occupy the central regions of the combustor, but are rather confined to peripheral regions of the combustor. This observation is in contrast to natural gas combustion in Figure 9(b) where the high temperature regions are concentrated in the central regions of the combustor. This can be attributed to the higher fuel velocity which causes the fuel jet to dominate over the

swirling air leading to lower mixing in the central regions of the combustor. However, like natural gas combustion, the high-temperature regions in biogas combustion increases with increasing swirl number and therefore increase in combustion efficiency can be expected with increasing swirl numbers.

The CO formation during biogas combustion shown in Figure 13(a) for the injector INJ-765 is quite different than in the natural gas combustion observed in Figure 11(a). For biogas, the CO formation is largely in two portions, first at the outer-IRZs and then at far downstream near the outlet whereas in natural gas combustion high concentrations of CO are located in the central regions of the combustor. With increasing swirl, the downstream CO formation increases and hence the higher CO emission at the combustor exit is expected. The NO formation trends for biogas combustion in Figure 13(b) follow patterns similar to that of natural gas in Figure 10(b) where the NO formation is observed mostly in the secondary and dilution zones of the combustor. The NO formation does not increase significantly with increasing swirl number for biogas combustion whereas for natural gas combustion a substantial increase in NO formation with higher swirl numbers is observed. The levels of NO emission for biogas are however much lower than that for natural gas.

All the trends in the contours of the biogas combustion in Figures 12-13 can be summarized as line plots as shown in Figure 14 to analyze the effect of the design parameters (injector diameter and swirl number) on the combustion performance optimization parameters (combustion efficiency, pattern factor, pollutant CO and NO emissions). The combustion efficiency in Figure 14(a) is found to be the highest for injector INJ-1065 whereas injector INJ-765, which was found to be most suitable for natural gas combustion shows lower efficiency. The pattern factor for injector INJ-1065 is also found to have the lowest values consistently and it does not show any significant change with increasing swirl numbers as depicted in Figure 14(b) (solid blue line).

Unlike the natural gas combustion results for CO and NO emissions (Figure 11(c)), the biogas combustion shows only a single intersecting point for the CO and NO lines at the X-axis location of S_g = 0.75 as shown in Figure 14(c). As the CO-NO lines are not intersecting for INJ-1065 and 575, therefore a balanced emission point for these two injectors cannot be identified clearly, although it appears that the lines for INJ-1065 may intersect at a swirl number less than 0.5 while an intersection point maybe achieved for a swirl number greater than 2.0 for INJ-575. It maybe noted furthermore from the trends of INJ-1065 and INJ-575 in Figure 14(d) that the combustion efficiency will be lower and the pattern factor will be higher for swirl numbers less than 0.5 which are undesirable. On the other hand, for swirl numbers greater than 2.0 the efficiency is likely to increase however NO emission is also expected to increase as can be predicted from Figure 14(c), thereby making injectors INJ-1065 and INJ-575 as not suitable options for biogas combustion. These observations are summarized in Table 5. Therefore, the intersection point of CO and NO emission at S_g = 0.75 representing the balanced emission for INJ-765 can be considered as the suitable trade-off

point for biogas combustion.

The key findings of the current investigations for both natural gas and biogas combustions can be summarized as follows:

- The injector INJ-765 can be considered a suitable choice for both natural gas and biogas combustions with S_g = 0.9 for natural gas and S_g = 0.75 for biogas combustion based on the suitable trade-off point identified for this injector.
- The best cases for the combustion optimization parameters are shown in Table 6.

It is essential to assess the comparative performance of natural gas and biogas, to determine the potential strengths and weaknesses of biogas for use in various industrial gas turbine engine applications as an alternative to traditional natural gas. The comparisons are shown in Figure 15.

The significant findings from the line plots in Figure 15 can be summed up as follows:

- INJ-765 with S_g = 0.75 for biogas combustion which has been identified as the suitable trade-off case, shows lower combustion efficiency (67.5%) as compared to suitable trade-off point for natural gas (92%) in Figure 15(a).
- Injector INJ-1065 with S_g = 2.0 for biogas combustion (dashed blue line) demonstrates combustion efficiency (Figure 15(a)) and heat generation (Figure 15(b)) comparable to natural gas despite having much lower amount of methane in biogas (65%) compared to natural gas (90%) and can be implemented in practical applications provided methods of reducing pollutant CO emissions can be developed, as the CO levels for biogas in the present combustor are higher than those for natural gas as observed in Figure 15(d).
- The suitable trade-off case for biogas combustion also demonstrates pattern factor values comparable to the suitable trade-off case for natural gas combustion in Figure 15(c). Additionally, with increasing swirl number the pattern factor for biogas reduces further and becomes similar to that for natural gas combustion for swirl number greater than 1.5. A similar trend of decreasing pattern factor, in the range 1.55 to 0.95 with increasing swirl number in the range 0.2 to 2.2 has been reported in published literature (Torkzadeh et al., 2016). Therefore, the current investigation seems to suggest that by increasing the swirl number, the pattern factor can be further reduced to lower recommended values ranging from 0.25 to 0.45 (Guoyu et al., 2014; Razak, 2007; Oates, 1989). Additionally, design changes such as modification of the dilution zone length and holes can lead to a more uniform temperature profile at the combustor outlet, lowering the pattern factor further.

- The main challenge and shortcoming of biogas combustion is excess CO emission compared to natural gas combustion as depicted in Figure 15(d), which needs to be controlled and reduced for biogas to be established as an industrial alternative fuel for use in gas turbine combustor applications.

- The NO emission is remarkably low during biogas combustion as shown in Figure 15(e), nevertheless, it is achieved at the expense of higher CO emission (Figure 15(d)).

Considering all these aspects, it can be observed that biogas has an immense potential in terms of its usage in industrial gas turbine applications as an alternative fuel to natural gas. Although the higher CO emission rate is the limitation for this combustion system, but the overall performance makes it a suitable candidate if the CO emission is controlled and reduced.

5. Conclusion

In the current work, the non-premixed combustion of the traditional fuel natural gas and the alternative fuel biogas were simulated in a swirling flow gas turbine combustor. To simulate the combustion, the standard $k-\epsilon$ and steady-flamelet models were used as the turbulence and turbulent-chemistry interaction models, respectively. The performances of natural gas and biogas combustion were analyzed based on multiple combustion performance optimization parameters and design parameters. Then the best swirl numbers and fuel injector diameter were identified for each combustion performance optimization parameters for both gases. Furthermore, a suitable trade-off case by considering all combustion performance optimization parameters has also been proposed, which are INJ-765 with S_g = 0.9 and INJ-765 with S_g = 0.75 for natural gas and biogas, respectively. It maybe noted here that the scaling of the Y_{NO} and Y_{CO} axis are somewhat arbitrary, although they were found not to effect the intersection points significantly. Therefore, it is recommended that a more suitable scaling for representing Y_{NO} and Y_{CO} maybe developed in a future work. Lastly, the combustion results are compared for both gases to assess the feasibility of using biogas in industrial gas turbines. The results indicate that the injector INJ-1065 with S_g = 2.0 for biogas of a specific composition gives performance similar to that of natural gas, although at the expense of higher CO emissions. Therefore, methods to reduce CO emissions will be targeted in a future work with focus on analyzing the influence of other design parameters including, but not limited to configuration of primary and secondary holes, and cooling slots in order to allow higher swirl numbers and thereby achieve lower pattern factors and higher efficiency of combustion for biogas. In addition, an investigation maybe carried out to study the influence of different biogas compositions with varying CH_4 and CO_2 amounts on flame stability, temperature distribution inside combustor, and pollutant emissions.

Acknowledgements

The authors gratefully acknowledge the computational facilities and support provided by the IIUM computational mechanics laboratory.

References

Al-Abdeli, Y. M. and Masri, A. R. (2003), 'Stability characteristics and flowfields of turbulent non-premixed swirling flames', *Combustion Theory and Modelling* **7**(4), 731–766.

Amani, E., Akbari, M. R. and Shahpouri, S. (2018), 'Multi-objective cfd optimizations of water spray injection in gas-turbine combustors', *Fuel* **227**, 267–278.

Amani, E., Rahdan, P. and Pourvosoughi, S. (2019), 'Multi-objective optimizations of air partitioning in a gas turbine combustor', *Applied Thermal Engineering* **148**, 1292–1302.

Ansari, M. and Amani, E. (2018), 'Micro-combustor performance enhancement using a novel combined baffle-bluff configuration', *Chemical Engineering Science* **175**, 243–256.

Arjmandi, H. R. and Amani, E. (2015), 'A numerical investigation of the entropy generation in and thermodynamic optimization of a combustion chamber', *Energy* **81**, 706–718.

Asgari, B. and Amani, E. (2017), 'A multi-objective cfd optimization of liquid fuel spray injection in dry-low-emission gas-turbine combustors', *Applied Energy* **203**, 696–710.

Bhoi, P. R. and Channiwala, S. A. (2008), 'Optimization of producer gas fired premixed burner', *Renewable Energy* **33**(6), 1209–1219.

Birouk, M., Saediamiri, M. and Kozinski, J. A. (2014), 'Non-premixed turbulent biogas flame: Effect of the co-airflow swirl strength on the stability limits', *Combustion Science and Technology* **186**(10), 1460–1477.

Biswas, W. K. (1994), Use of biogas as diesel engine fuel, Master's thesis, Department of Mechanical Engineering, Bangladesh University of Engineering and Technology, Dhaka, Bangladesh.

Bothien, M. R., Ciani, A., Wood, J. P. and Fruechtel, G. (2019), 'Toward decarbonized power generation with gas turbines by using sequential combustion for burning hydrogen', *Journal of Engineering for Gas Turbines and Power* **141**(12), 121013.

Boyce, M. P. (2012), *Gas Turbine Engineering Handbook*, 4th edn, Elsevier Inc., Waltham, MA.

Burmberger, S. and Sattelmayer, T. (2011), 'Optimization of the aerodynamic flame stabilization for fuel flexible gas turbine premix burners', *Journal of Engineering for Gas Turbines and Power* **133**(10), 101501.

Chen, J., Wang, Y., Liu, H. and Weng, Y. (2017), 'Experimental study of flow characteristics of enhanced biogas lean premixed nozzle of micro gas turbine by piv', *Applied Thermal Engineering* **121**, 90–102.

Chmielewski, M. and Gieras, M. (2017), 'Impact of variable geometry combustor on performance and emissions from miniature gas turbine engine', *Fuel* **90**(2), 257–264.

Conrado, A. C., Lacava, P. T., Filho, A. C. P. and de Souza Sanches, M. (2004), Basic design principles for gas turbine combustor, *in* 'Proceedings of the 10th Brazilian Congress of Thermal Sciences and Engineering - ENCIT 2004', 29 November-3 December 2004, Rio de Janeiro, Brazil.

Şahin, M. (2019), 'Combustion characteristics of various biogas flames under reduced oxygen concentration conditions', *Energy Sources, Part A: Recovery, Utilization, and Environmental Effects* **41**(19), 2415–2427.

Şahin, M. and İlbaş, M. (2019), 'Analysis of the effect of h20 content on combustion behaviours of a biogas fuel', *International Journal of Hydrogen Energy* .

Effuggi, A., Gelosa, D., Derudi, M. and Rota, R. (2008), 'Mild combustion of methane-derived fuel mixtures: Natural gas and biogas', *Combustion Science and Technology* **180**(3), 481–493.

Elbaz, A. M. and Roberts, W. L. (2016), 'Investigation of the effects of quarl and initial conditions on swirling non-premixed methane flames: Flow field, temperature, and species distributions', *Fuel* **169**, 120–134.

Elbaz, A. M., Yu, S., Liu, X., Bai, X. S., Khesho, I. and Roberts, W. L. (2019), 'An experimental/numerical investigation of the role of the quarl in enhancing the blowout limits of swirl-stabilized turbulent non-premixed flames', *Fuel* **236**, 1226–1242.

Emami, M. D., Shahbazian, H. and Sunden, B. (2019), 'Effect of operational parameters on combustion and emissions in an industrial gas turbine combustor', *Journal of Engineering for Gas Turbines and Power* **141**(1), 012202.

Farokhipour, A., Hamidpour, E. and Amani, E. (2018), 'A numerical study of nox reduction by water spray injection in gas turbine combustion chambers', *Fuel* **212**, 173–186.

Fischer, M. and Jiang, X. (2015), 'An investigation of the chemical kinetics of biogas combustion', *Fuel* **150**, 711–720.

Fischer, M. and Jiang, X. (2017), 'Numerical studies of co formation during biogas combustion', *Energy Procedia* **142**, 426–431.

Fuligno, L., Micheli, D. and Poloni, C. (2009), 'An integrated approach for optimal design of micro gas turbine combustors', *Journal of Thermal Science* **18**(2), 173–184.

Gökalp, I. and Lebas, E. (2004), 'Alternative fuels for industrial gas turbines (aftur)', *Applied Thermal Engineering* **24**(11), 1655–1663.

Göke, S., Schimek, S., Terhaar, S., Reichel, T., Göckeler, K., Krüger, O., Fleck, J., Griebel, P. and Paschereit, C. O. (2014), 'Influence of pressure and steam dilution on nox and co emissions in a premixed natural gas flame', *Journal of Engineering for Gas Turbines and Power* **136**(9), 091508.

Guessab, A., Aris, A., Cheikh, M. and Baki, T. (2016), 'Combustion of methane and biogas fuels in gas turbine can-type combustor model', *Journal of Applied Fluid Mechanics* **9**(5), 2229–2238.

Guoyu, D., Xiaomin, H., Ziqiang, Z., Bokun, A., Yaoyu, S. and Yixiao, Z. (2014), 'Effect of dilution holes on the performance of a triple swirler combustor', *Chinese Journal of Aeronautics* **27**(6), 1421–1429.

Hajitaheri, S. (2012), Design optimization and combustion simulation of two gaseous and liquid-fired combustors, Master's thesis, Department of Mechanical Engineering, University of Waterloo, Waterloo, Ontario, Canada.
URL: *http://hdl.handle.net/10012/6730*

Heywood, J. B. (1988), *Internal combustion engine fundamentals*, McGraw-Hill series in mechanical engineering, McGraw-Hill, Inc.
Hobson, P. N., Bousfield, S. and Summers, R. (1981), *Methane Production from Agricultural and Domestic Wastes*, Energy from Wastes series, 1st edn, Applied Science Publishers Limited, London.
Hosseini, S. E., Bagheri, G. and Wahid, M. A. (2014), 'Numerical investigation of biogas flameless combustion', *Energy Conversion and Management* **81**, 41–50.
Hosseini, S. E. and Wahid, M. A. (2013), 'Biogas utilization: Experimental investigation on biogas flameless combustion in lab-scale furnace', *Energy Conversion and Management* **74**, 426–432.
Hosseini, S. E. and Wahid, M. A. (2014), 'Development of biogas combustion in combined heat and power generation', *Renewable and Sustainable Energy Reviews* **40**, 868–875.
Hosseini, S. E. and Wahid, M. A. (2015), 'Effects of burner configuration on the characteristics of biogas flameless combustion', *Combustion Science and Technology* **187**(8), 1240–1262.
Iki, N., Gruber, A. and Yoshida, H. (2007), Anumerical and an experimental study for optimization of a small annular combustor, *in* 'Challenges of Power Engineering and Environment', Berlin, Heidelberg, pp. 1429–1435.
İlbaş, M. and Şahin, M. (2017), 'Effects of turbulator angle and hydrogen addition on a biogas turbulent diffusion flame', *International Journal of Hydrogen Energy* **42**(40), 25735–25743.
İlbaş, M., Şahin, M. and Karyeyen, S. (2016), 'Combustion behaviours of different biogases in an existing conventional natural gas burner: An experimental study', *International journal of renewable energy research* **6**(3), 1178–1188.
ΩİIbaş et al.
İlbaş, M., Şahin, M. and Karyeyen, S. (2018), '3d numerical modelling of turbulent biogas combustion in a newly generated 10 kw burner', *Journal of the Energy Institute* **91**(1), 87–99.
İlbaş, M., Karyeyen, S. and İlker Yılmaz (2016), 'Effect of swirl number on combustion characteristics of hydrogen-containing fuels in a combustor', *International Journal of Hydrogen Energy* **41**(17), 7185–7191.
İlker Yılmaz (2013), 'Effect of swirl number on combustion characteristics in a natural gas diffusion flame', *Journal of Energy Resources Technology* **135**(4), 042204.
Iqbal, S., Benim, A. C., Fischer, S., Joos, F., Kluß, D. and Wiedermann, A. (2016), 'Experimental and numerical analysis of natural bio and syngas swirl flames in a model gas turbine combustor', *Journal of Thermal Science* **25**(5), 460–469.
ISO (1995), Natural gas – Calculation of calorific values, density, relative density and Wobbe index from composition, Standard, International Organization for Standardization, Geneva, CH.
Janiga, G. and Thévenin, D. (2007), 'Reducing the co emissions in a laminar burner using different numerical optimization methods', *Proceedings of the Institution of Mechanical Engineers, Part A: Journal of Power and Energy* **221**(5), 647–655.
Jaravel, T. (2016), Prediction of pollutants in gas turbines using Large Eddy Simulation, Doctoral dissertation, École doctorale Mécanique, Energtique, Génie Civil et Procédés, Université de Toulouse, Toulouse, France.
Jerzak, W. and Kuźnia, M. (2016), 'Experimental study of impact of swirl number as well as oxygen and carbon dioxide content in natural gas combustion air on flame flashback and blow-off', *Journal of Natural Gas Science and Engineering* **29**, 46–54.
Kahraman, N., Tangöz, S. and Akansu, S. O. (2018), 'Numerical analysis of a gas turbine combustor fueled by hydrogen in comparison with jet-a fuel', *Fuel* **217**, 66–77.
Kalt, P. A. M., Al-Abdeli, Y. M., Masri, A. R. and Barlow, R. S. (2002), 'Swirling turbulent non-premixed flames of methane: Flow field and compositional structure', *Proceedings of the Combustion Institute* **29**(2), 1913–1919.
Khaleghi, M., Hosseini, S. E. and Wahid, M. A. (2015), 'Experimental and numerical investigations of biogas vortex combustion', *Proceedings of the Institution of Mechanical Engineers, Part A: Journal of Power and Energy* **229**(6), 662–676.
Krieger, G. C., Campos, A. P. V., Takehara, M. D. B., da Cunha, F. A. and Veras, C. A. G. (2015), 'Numerical simulation of oxy-fuel combustion for gas turbine applications', *Applied Thermal Engineering* **78**, 471–481.
Kuznetsov, N. V., ed. (1973), *Standard Methods of Thermal Design for Power Boilers*, Energiya, Moscow.
Lam, C. K. G. and Bremhorst, K. (1981), 'A modified form of the k-ϵ model for predicting wall turbulence', *Journal of Fluids Engineering* **103**(3), 456–460.
Launder, B. E. and Spalding, D. B. (1974), 'The numerical computation of turbulent flows', *Computer Methods in Applied Mechanics and Engineering* **3**(2), 269–289.
Lefebvre, A. H. and Ballal, D. R. (2010), *Gas Turbine Combustion: Alternative Fuels and Emissions*, 3rd edn, CRC Press- Taylor & Francis Group, Boca Raton, FL.
Lellek, S., Barfuß, C. and Sattelmayer, T. (2017), 'Experimental study of the interaction of water sprays with swirling premixed natural gas flames', *Journal of Engineering for Gas Turbines and Power* **139**(2), 021506.
Leung, T. and Wierzba, I. (2007), Stability limits of biogas jet diffusion flames, Vol. Volume 6: Energy Systems: Analysis, Thermodynamics and Sustainability of *ASME International Mechanical Engineering Congress and Exposition*, pp. 65–73.
Leung, T. and Wierzba, I. (2008), 'The effect of hydrogen addition on biogas non-premixed jet flame stability in a co-flowing air stream', *International Journal of Hydrogen Energy* **33**(14), 3856–3862.
Li, L., Lin, Y., Fu, Z. and Zhang, C. (2016), 'Emission characteristics of a model combustor for aero gas turbine application', *Experimental Thermal and Fluid Science* **72**, 235–248.
Liguori, V. (2016), 'Numerical investigation: Performances of a standard biogas in a 100 kwe mgt', *Energy Reports* **2**, 99–106.
Makhanlall, D., Munda, J. L. and Jiang, P. (2013), 'Radiation energy devaluation in diffusion combusting flows of natural gas', *Energy* **61**, 657–63.
Masri, A. R. (2007), 'Sydney swirl flows and flames database', http://web.aeromech.usyd.edu.au/thermofluids/swirl.php.
Masri, A. R. (2020), 'Challenges for turbulent combustion (in press)', *Proceedings of the Combustion Institute* .
Mattingly, J. D., Heiser, W. H. and Pratt, D. T. (2002), *Aircraft engine design*, AIAA Education Series, 2nd edn, American Institute of Aeronautics and Astronautics, Inc., Reston, VA.
Melconian, J. O. and Modak, A. T. (1985), Combustor design, *in* J. W. Sawyer, ed., 'Sawyer's Gas Turbine Engineering Handbook: Theory and Design', Vol. 1, Turbomachinery International Publications, Connecticut, chapter 5, pp. 1–62.

Mordaunt, C. J. and Pierce, W. C. (2014), 'Design and preliminary results of an atmospheric-pressure model gas turbine combustor utilizing varying co2 doping concentration in ch4 to emulate biogas combustion', *Fuel* **124**, 258–268.
Motsamai, O. S., Snyman, J. A. and Meyer, J. P. (2010), 'Optimization of gas turbine combustor mixing for improved exit temperature profile', *Heat Transfer Engineering* **31**(5), 402–418.
Murphy, C. M. (2004), Design and construction of a gas turbine combustor test rig for alternative fuel testing, Master's thesis, Department of Mechanical and Aerospace Engineering, Carleton University, Ottawa, Ontario, Canada.
Oates, G. C., ed. (1989), *Aircraft Propulsion Systems Technology and Design*, AIAA Education Series, American Institute of Aeronautics and Astronautics, Inc., Washington, DC.
Patankar, S. V. (1980), *Numerical Heat Transfer and Fluid Flow*, Computational Methods in Mechanics and Thermal Sciences, 1st edn, Hemisphere Publishing Corporation, Washington.
Peters, N. (2004), *Turbulent Combustion*, Cambridge Monographs on Mechanics, Cambridge University Press.
Pitsch, H. and Peters, N. (1998), 'A consistent flamelet formulation for non-premixed combustion considering differential diffusion effects', *Combustion and Flame* **114**(1), 26–40.
Poinsot, T. and Veynante, D. (2005), *Theoretical and Numerical Combustion*, 2nd edn, R. T. Edwards, Inc., Philadelphia, PA.
Rajabi, V. and Amani, E. (2018), 'A computational study of swirl number effects on entropy generation in gas turbine combustors', *Heat Transfer Engineering* **40**(3), 346–361.
Rashwan, S. S., Habib, M. A., Ben-Mansour, R., Nemitallah, M. A. and Abdelhafez, A. (2018), 'The effect of swirl number and oxidizer composition on combustion characteristics of non-premixed methane flames', *Energy & Fuels* **32**(4), 5664–5664.
Razak, A. M. Y. (2007), *Industrial gas turbines: Performance and operability*, Woodhead Publishing Limited and CRC Press LLC, Cambridge, England.
Rohani, B. and Saqr, K. M. (2012), 'Effects of hydrogen addition on the structure and pollutant emissions of a turbulent unconfined swirling flame', *International Communications in Heat and Mass Transfer* **39**(5), 681–688.
Saediamiri, M., Birouk, M. and Kozinski, J. A. (2016), 'Enhancing the stability limits of biogas non-premixed flame', *Combustion Science and Technology* **188**(11), 2077–2104.
Safer, K., Ouadha, A. and Tabet, F. (2017), 'Entropy generation in turbulent syngas counter-flow diffusion flames', *International Journal of Hydrogen Energy* **42**(49), 29532–29544.
Sahebjamei, M., Amani, E. and Nobari, M. R. H. (2019), 'Numerical analysis of radial and angular stratification in turbulent swirling flames', *Energy* **173**, 523–539.
Santhosh, R. and Basu, S. (2016), 'Transitions and blowoff of unconfined non-premixed swirling flame', *Fuel* **164**, 135–152.
Sayre, A., Lallemant, N., Dugue, J. and Weber, R. (1994), Scaling characteristics of the aerodynamics and low nox properties of industrial natural gas burners scaling 400 study. part 4. 300 kw berl test results, Topical report, International Flame Research Foundation, Ijmuiden, Netherlands.
Shahpouri, S. and Houshfar, E. (2019), 'Nitrogen oxides reduction and performance enhancement of combustor with direct water injection and humidification of inlet air', *Clean Technologies and Environmental Policy* **21**(3), 667–683.
Shanbhogue, S. J., Sanusi, Y. S., Taamallah, S., Habib, M. A., Mokheimer, E. M. A. and Ghoniem, A. F. (2016), 'Flame macrostructures, combustion instability and extinction strain scaling in swirl-stabilized premixed ch4/h2 combustion', *Combustion and Flame* **163**, 494–507.
Sivathanu, Y. R. and Faeth, G. M. (1990), 'Generalized state relationships for scalar properties in nonpremixed hydrocarbon/air flames', *Combustion and Flame* **82**(2), 211–230.
Taamallah, S., Shanbhogue, S. J. and Ghoniem, A. F. (2016), 'Turbulent flame stabilization modes in premixed swirl combustion: Physical mechanism and karlovitz number-based criterion', *Combustion and Flame* **166**, 19–33.
Torkzadeh, M. M., Bolourchifard, F. and Amani, E. (2016), 'An investigation of air-swirl design criteria for gas turbine combustors through a multi-objective cfd optimization', *Fuel* **186**, 734–749.
Wankhede, M. J., Bressloff, N. W. and Keane, A. J. (2011), 'Combustor design optimization using co-kriging of steady and unsteady turbulent combustion', *Journal of Engineering for Gas Turbines and Power* **133**(12), 121504.
Yang, X., He, Z., Qiu, P., Dong, S. and Tan, H. (2019), 'Numerical investigations on combustion and emission characteristics of a novel elliptical jet-stabilized model combustor', *Energy* **170**, 1082–1097.
Zhang, Z., Liu, X., Gong, Y., Li, Z., Yang, J. and Zheng, H. (2020), 'Investigation on flame characteristics of industrial gas turbine combustor with different mixing uniformities', *Fuel* **259**, 116297.
Zhen, H. S., Leung, C. W. and Cheung, C. S. (2013), 'Effects of hydrogen addition on the characteristics of a biogas diffusion flame', *International Journal of Hydrogen Energy* **38**(16), 6874–6881.
Zhen, H. S., Leung, C. W. and Cheung, C. S. (2014), 'A comparison of the heat transfer behaviors of biogash2 diffusion and premixed flames', *International Journal of Hydrogen Energy* **39**(2), 1137–1144.
Zhen, H. S., Leung, C. W., Cheung, C. S. and Huang, Z. H. (2014), 'Characterization of biogas-hydrogen premixed flames using bunsen burner', *International Journal of Hydrogen Energy* **39**(25), 13292–13299.

Table 1: Specification of the combustor.

	Combustor specification	Value
$\dot{m}_{fuel}$	Fuel flow rate (natural gas)	0.0323 kg/s
$\dot{Q}_{fuel}$	Lower heating value (natural gas)	48.24 MJ/kg (ISO, 1995)
$\dot{m}_{fuel} \times \dot{Q}_{fuel}$	Estimated heat generation (natural gas)	1.558 MJ/s
$\dot{m}_{fuel}$	Fuel flow rate (biogas)	0.0797 kg/s
$\dot{Q}_{fuel}$	Lower heating value (biogas)	20.43 MJ/kg (Gökalp and Lebas, 2004; ISO, 1995)
$\dot{m}_{fuel} \times \dot{Q}_{fuel}$	Estimated heat generation (biogas)	1.628 MJ/s
R_f	Fuel injector radius (INJ-765)	7.65 mm
T_f	Inlet fuel temperature	500 K
$\dot{m}_3$	Total inlet air	1.9177 kg/s
S_g	Empirical swirl number	0.9
θ	Swirl angle	48°
T_3	Inlet air temperature	543.43 K
P_3	Inlet air pressure	8.106 bar

Table 2: Compositions (by mole fraction) of gases used in current study.

Species	Natural Gas	Biogas
CH_4	90%	65%
C_2H_6	8.5%	-
CO_2	0.5%	33%
N_2	1%	1.3%
O_2	-	0.7%

Table 3: Fuel injectors used as design parameter in current work.

Injector	Radius	Diameter	Relative diameter	Separator between swirler and injector	Thickness of the separator
INJ-1065	10.65 mm	21.3 mm	100%	Wall	0.75 mm
INJ-765	7.65 mm	15.3 mm	70%	Bluff-body	3.75 mm
INJ-575	5.75 mm	11.5 mm	50%	Bluff-body	5.65 mm

Table 4: Combustion efficiency and pattern factor for swirl numbers corresponding to balanced emissions for natural gas combustion.

Injector	Swirl number	Combustion Efficiency	Pattern Factor
INJ-1065	0.755	0.89	1.55
INJ-765	0.898	0.92	1.5
INJ-575	1.215	0.9	1.5

Table 5: Combustion Efficiency and pattern factor for swirl numbers corresponding to balanced emissions for biogas combustion.

Injector	Swirl number	Combustion Efficiency	Pattern Factor
INJ-1065	NA	NA	NA
INJ-765	0.75	0.68	1.54
INJ-575	NA	NA	NA

Table 6: Best cases for different combustion performance optimization parameters.

Optimization parameters	**Natural Gas**	**Biogas**
Combustion efficiency	INJ-765 with $S_g = 2.0$	INJ-1065 with $S_g = 2.0$
Pattern factor	INJ-765 with $S_g = 2.0$	INJ-765 with $S_g = 2.0$
Balanced emission	INJ-765 with $S_g = 0.9$	INJ-765 with $S_g = 0.75$

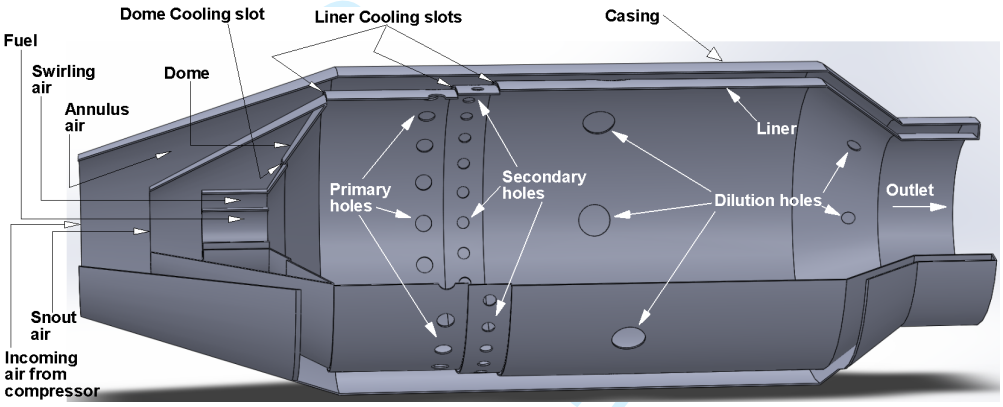

Figure 1: Cutout geometry of the combustor.

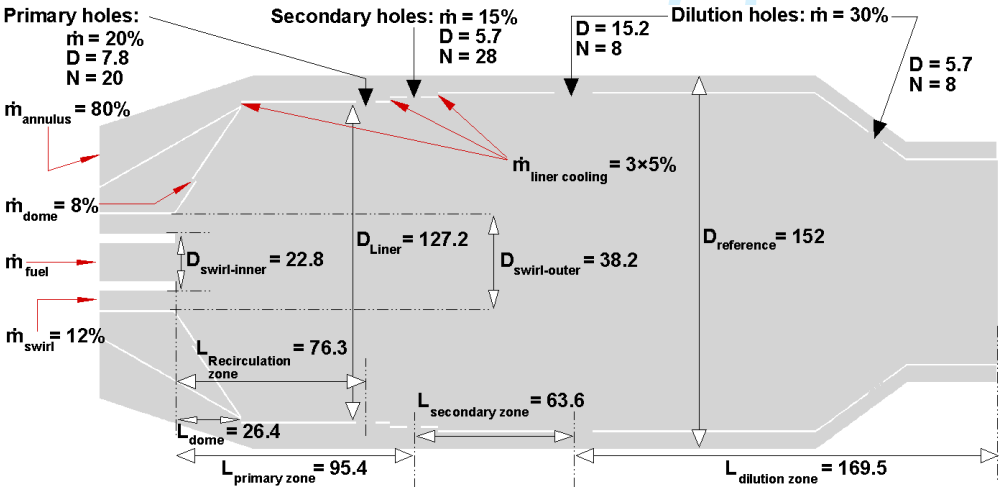

Figure 2: Cross-sectional view of the computational domain with various dimensions (in millimeter) and flow rates (as percentage of total air), for the specifications given in Table 1. D = diameter, $\dot{m}$ = mass flow rate, L = length, N = number of holes.

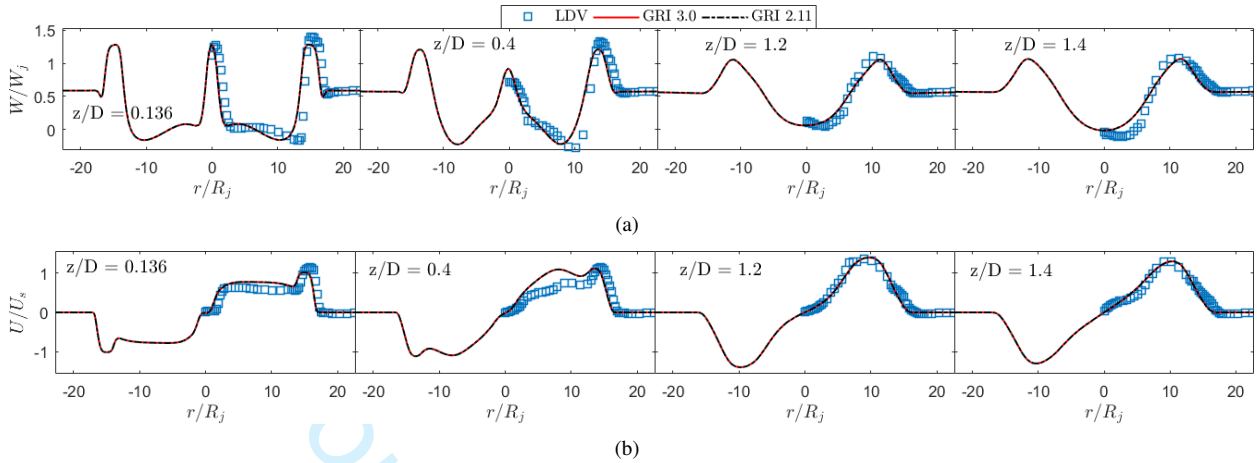

Figure 3: (a) Axial and (b) tangential velocity versus radial distance at centerline YZ-plane with different distances from inlet. Comparison between experimental measurements (LDV) (Kalt et al., 2002; Masri, 2007) and computation using GRI 3.0 and 2.11 mechanisms.

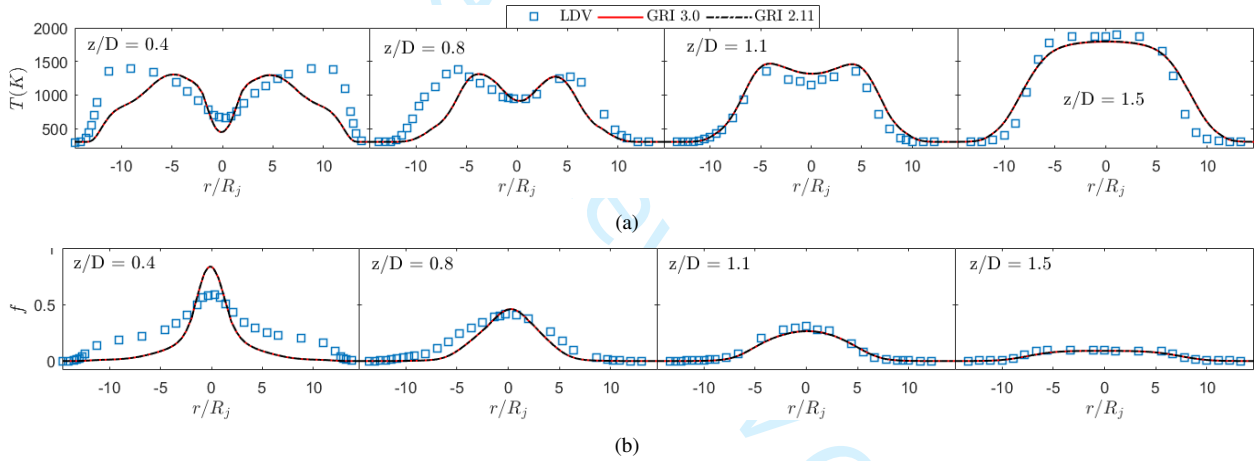

Figure 4: (a) Temperature and (b) mean mixture fraction versus radial distance at centerline YZ-plane with different distances from inlet. Comparison between experimental measurements (LDV) (Kalt et al., 2002; Masri, 2007) and computation using GRI 3.0 and 2.11 mechanisms.

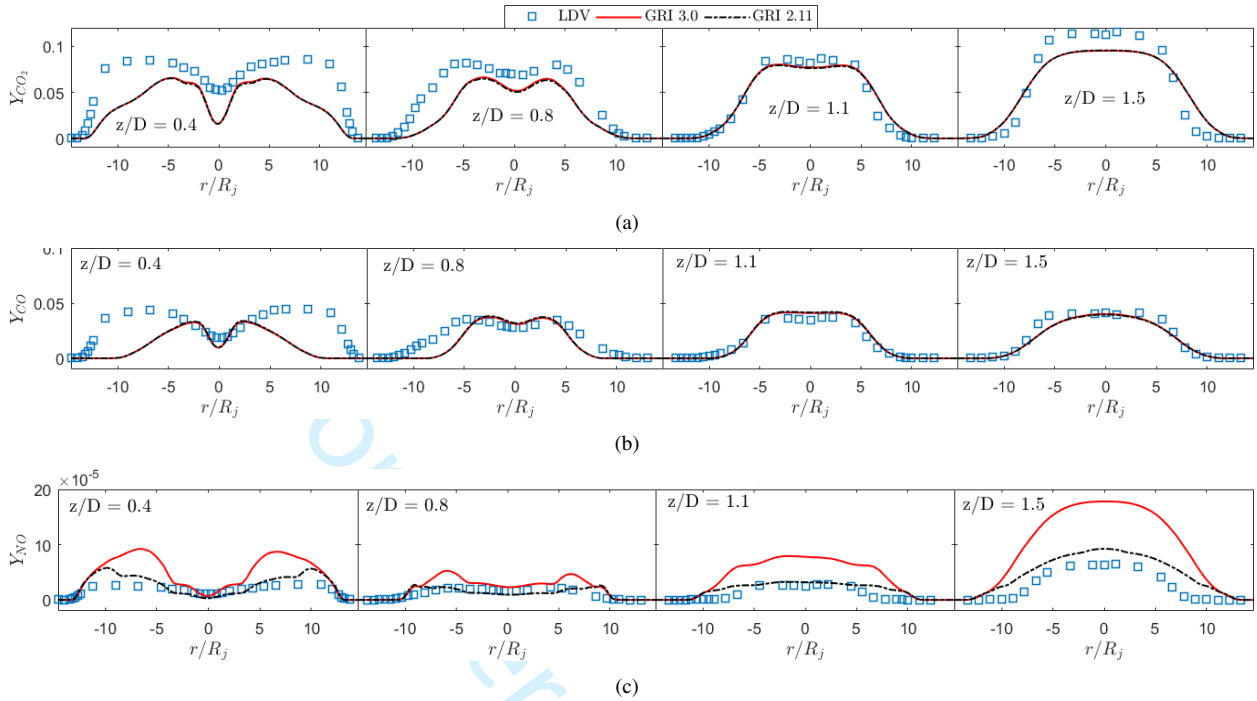

Figure 5: (a) CO_2, (b) CO, and (c) NO mass fraction versus radial distance at centerline YZ-plane with different distances from inlet. Comparison between experimental measurements (LDV) (Kalt et al., 2002; Masri, 2007) and computation using GRI 3.0 and 2.11 mechanisms.

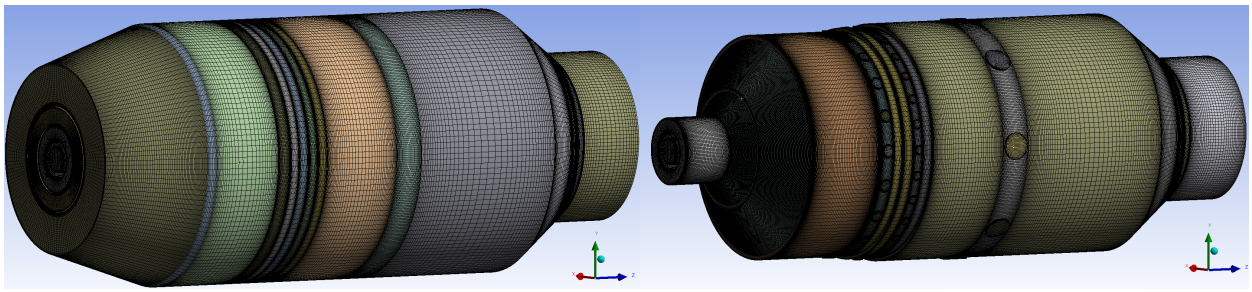

(a) The grid with annulus (left) and without annulus (right).

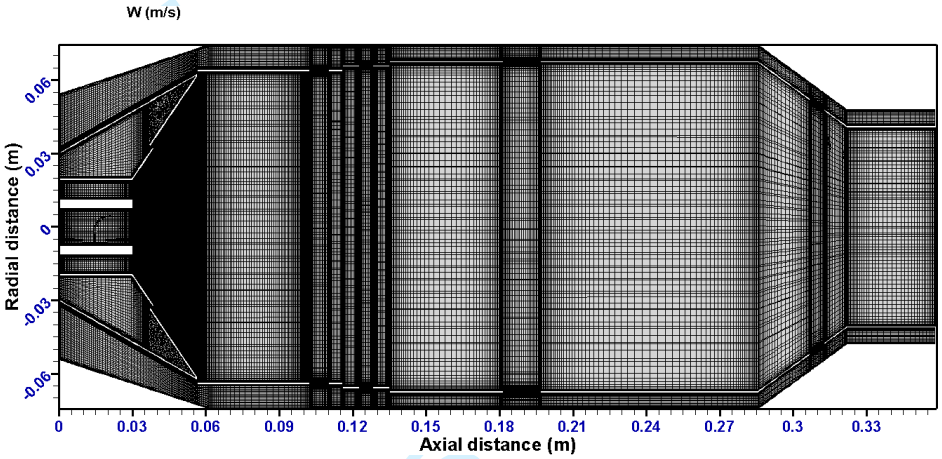

(b) Grid structure at the centerline YZ-plane.

Figure 6: Grid of the combustor.

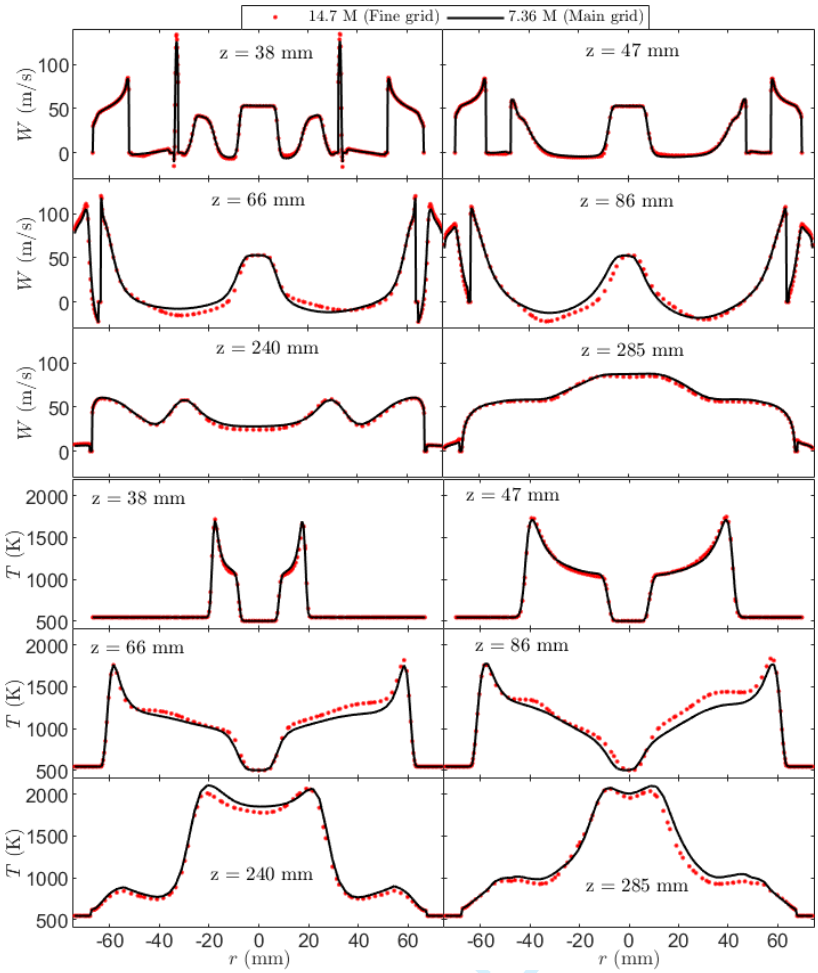

Figure 7: Axial velocity (top) and temperature (bottom) versus radial distance at centerline YZ-plane with distances from inlet. Comparison between computation using main and finer mesh.

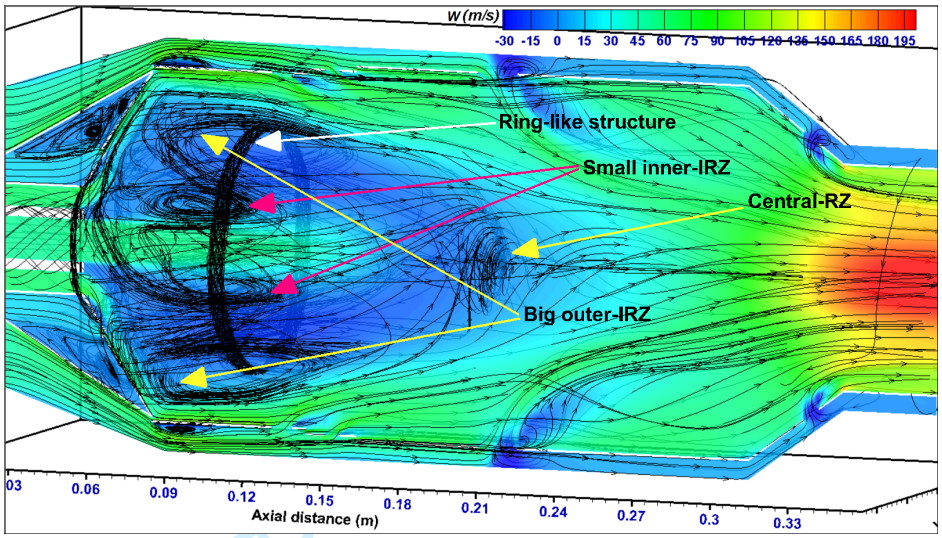

(a)

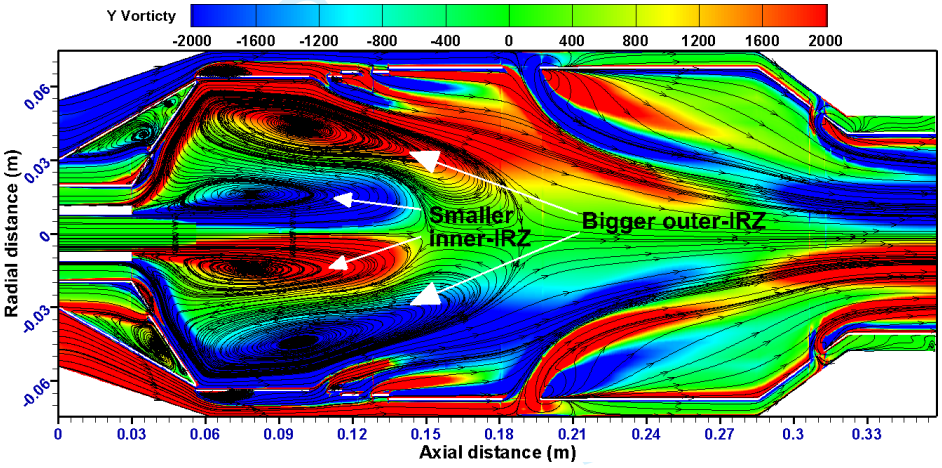

(b)

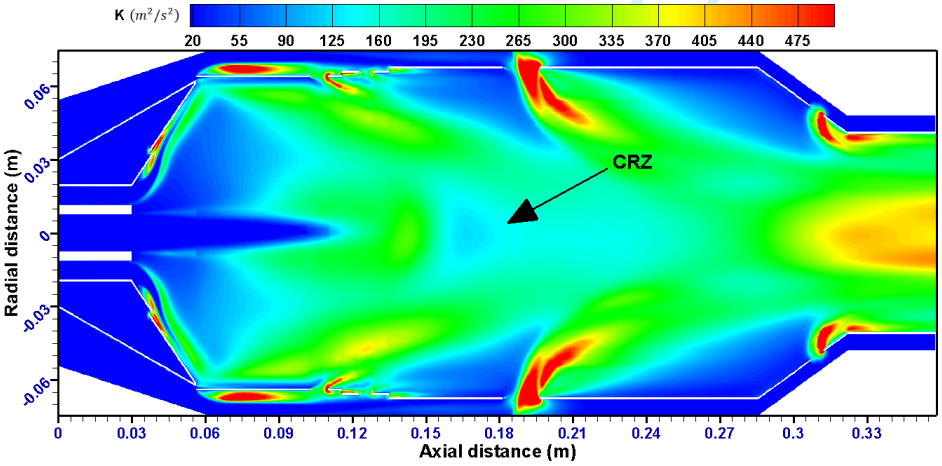

(c)

Figure 8: Contours of the reference case (INJ-765 with S_g = 0.9): (a) 3D streamlines along with a translucent slice of the axial velocity contour at the centerline of the 3D domain, (b) Y-vorticity with 2D streamlines, (c) turbulent kinetic energy.

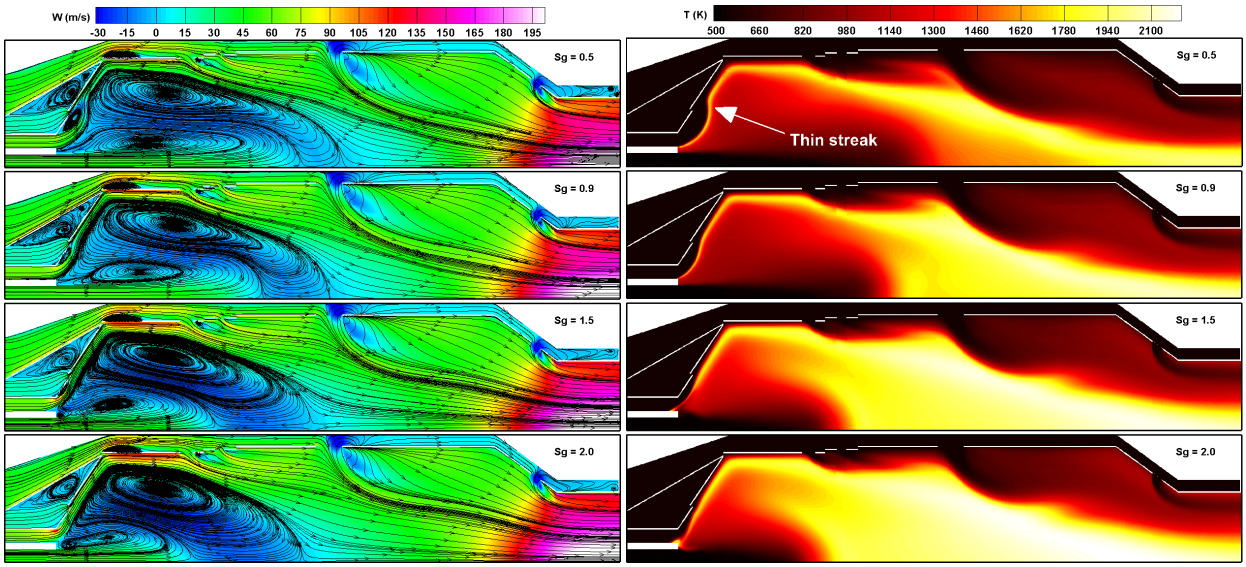

(a) (b)

Figure 9: Contours of (a) axial velocity with 2D streamlines; (b) temperature; for INJ-765 with different swirl numbers for natural gas combustion.

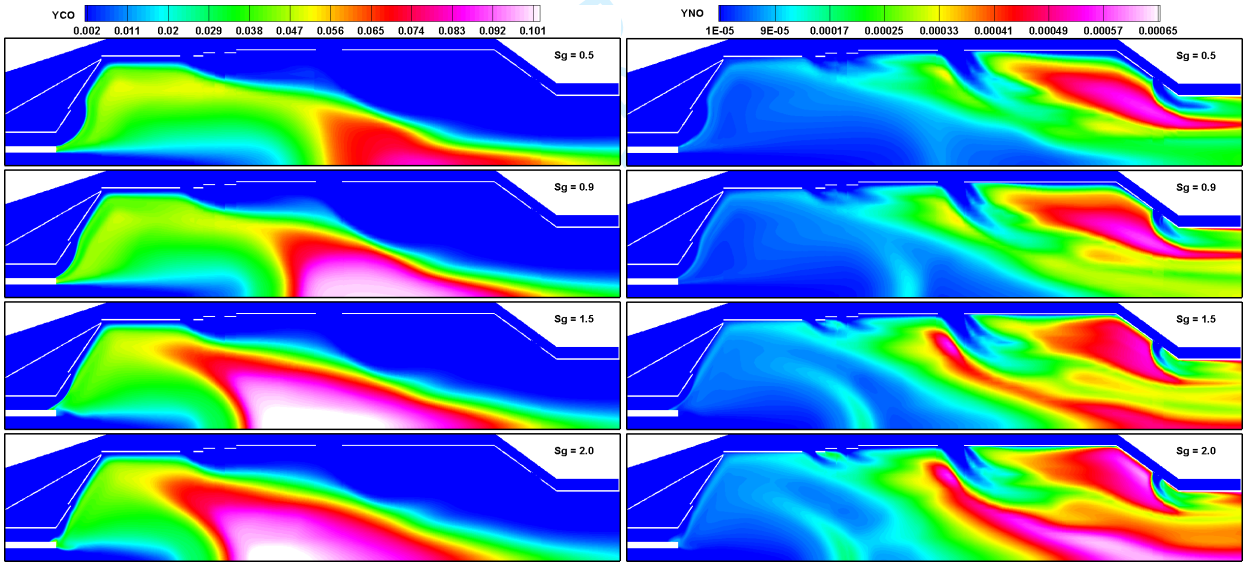

(a) (b)

Figure 10: Contours of (a) CO and (b) NO mass fraction for INJ-765 with different swirl numbers for natural gas combustion.

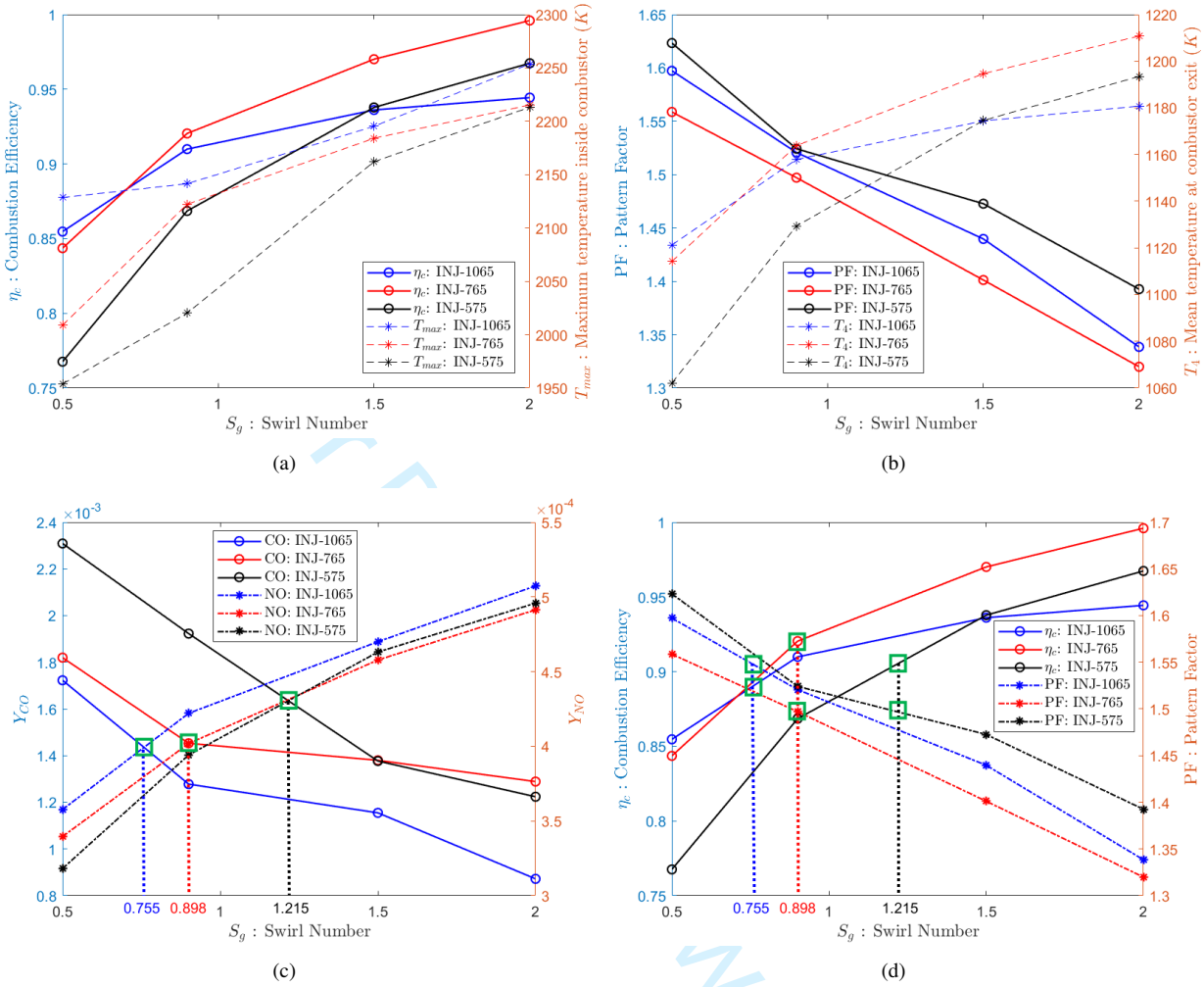

Figure 11: Natural gas combustion cases for all fuel injectors and against swirl numbers: (a) combustion efficiency and maximum combustor temperature; (b) pattern factor and mean temperature at the combustor exit; (c) CO and NO emission through the combustor exit; (d) combustion efficiency and pattern factor.

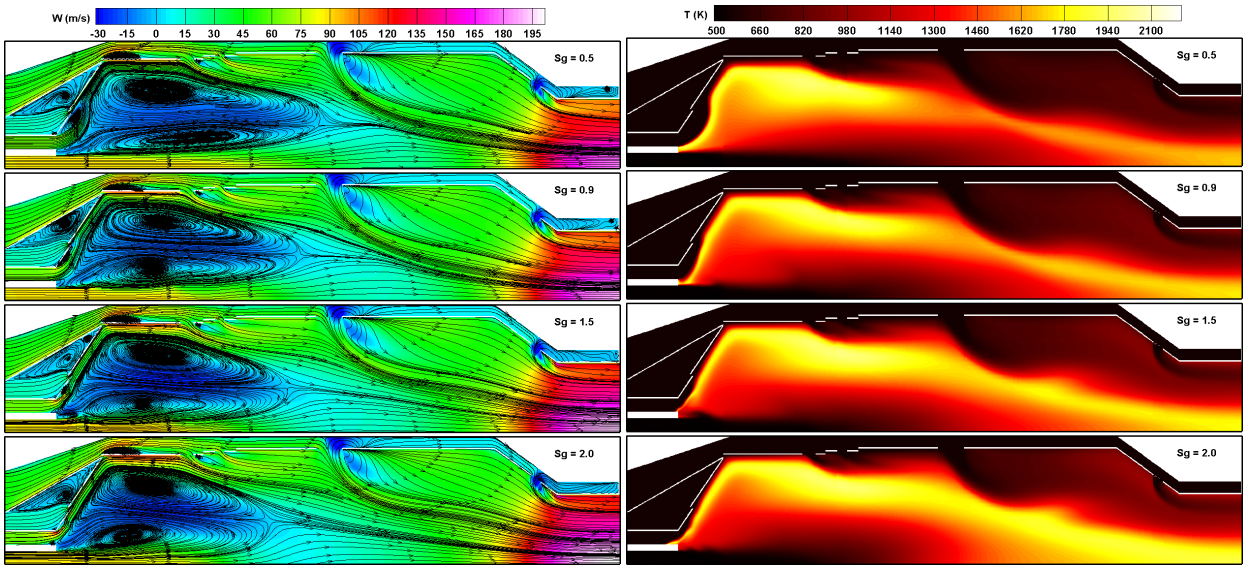

(a) (b)

Figure 12: Contours of (a) axial velocity with 2D streamlines; (b) temperature; for INJ-765 with different swirl numbers for biogas combustion.

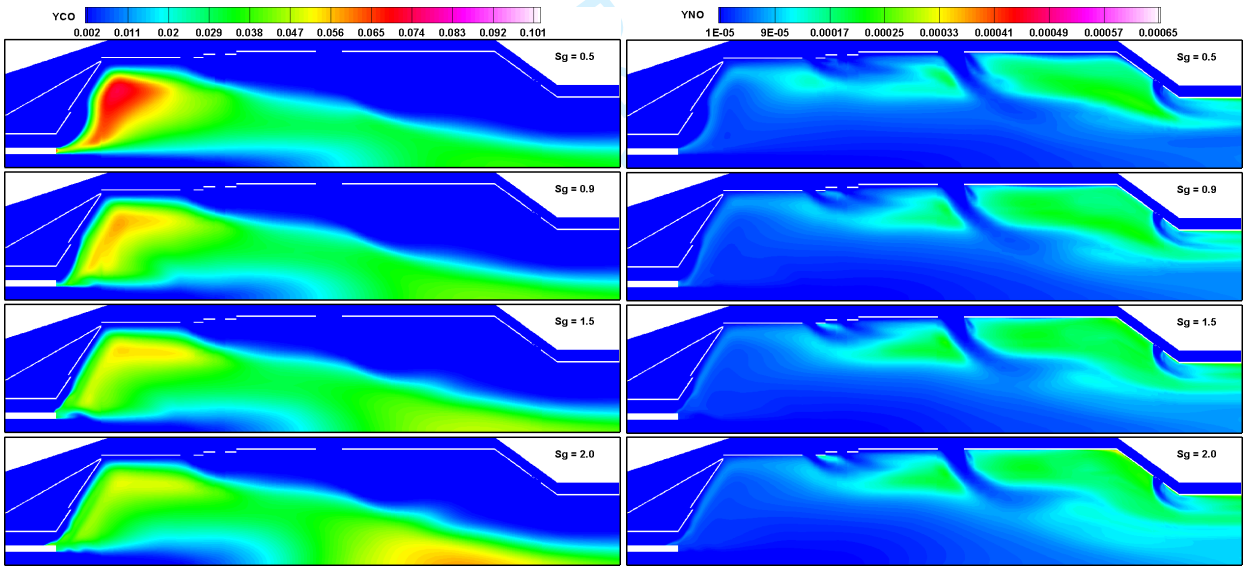

(a) (b)

Figure 13: Contours of (a) CO and (b) NO mass fraction for INJ-765 with different swirl numbers for biogas combustion.

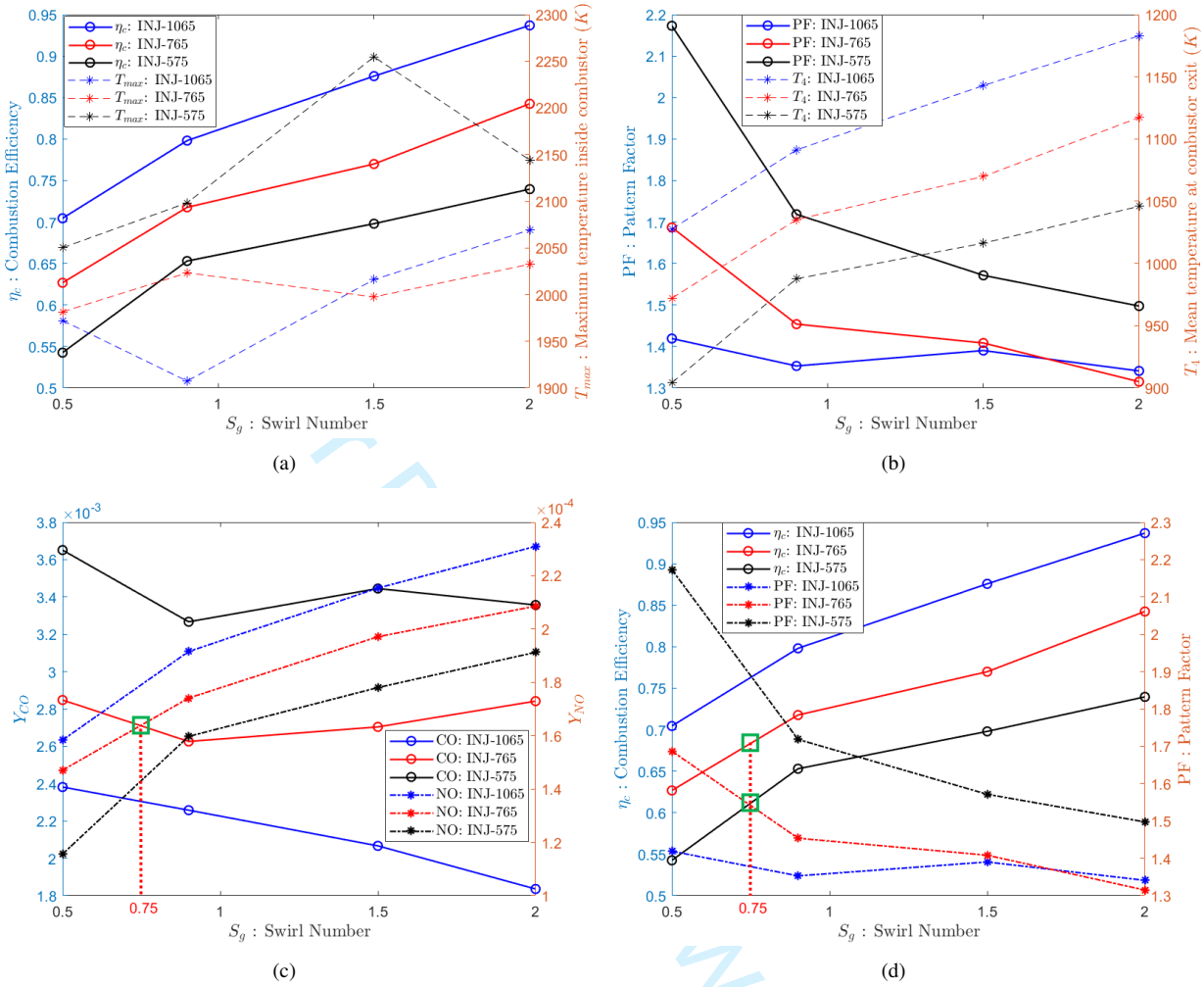

Figure 14: Biogas combustion cases for all fuel injectors and against swirl numbers: (a) combustion efficiency and maximum temperature inside combustor; (b) pattern factor and mean temperature at combustor exit; (c) CO and NO emission through combustor exit; (d) combustion efficiency and pattern factor.

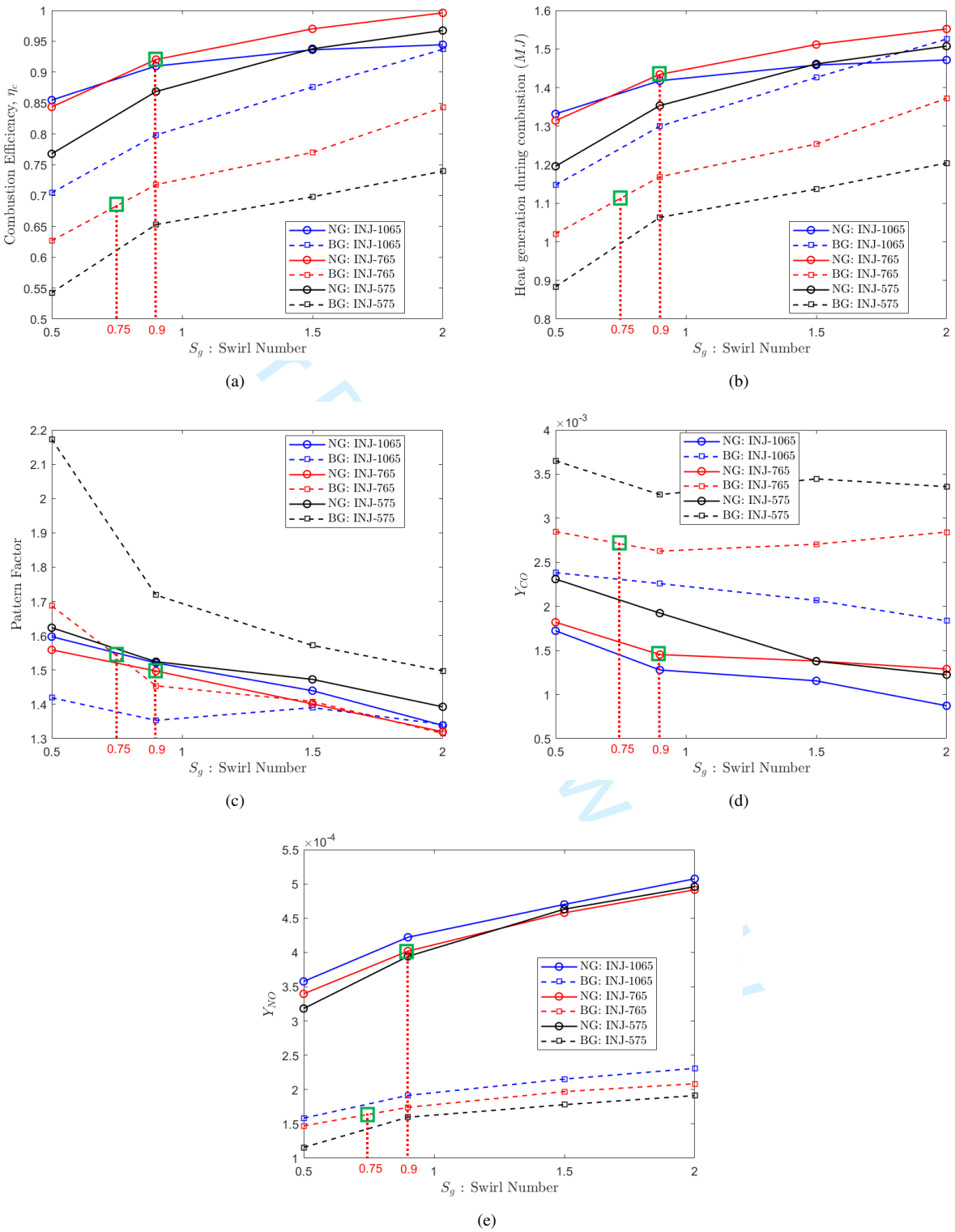

Figure 15: Comparative performance analysis of natural gas (NG) and biogas (BG) combustion with suitable trade-off cases indicated by green squares: (a) combustion efficiency, (b) combustion heat generation, (c) pattern factor, (d) CO emission, (e) NO emission at the combustor exit against swirl number and for all fuel injectors.